Phys. Status Solidi B **250**, No. 6, 1191–1203 (2013) / **DOI** 10.1002/pssb.201248370

Part of Special Issue on
Metal–Substrate Interactions in Heterogeneous Catalysis

physica status solidi b
www.pss-b.com
basic solid state physics

Feature Article

Neural network potentials for metals and oxides – First applications to copper clusters at zinc oxide

Nongnuch Artrith, Björn Hiller, and Jörg Behler*

Lehrstuhl für Theoretische Chemie, Ruhr-Universität Bochum, 44780 Bochum, Germany

Received 10 August 2012, revised 24 October 2012, accepted 30 October 2012
Published online 6 December 2012

Keywords copper, heterogeneous catalysis, interatomic potentials, molecular dynamics simulations, neural networks, ZnO

* Corresponding author: e-mail joerg.behler@theochem.rub.de, Phone: +49-234-3226749, Fax: +49-234-3214045

The development of reliable interatomic potentials for large-scale molecular dynamics (MD) simulations of chemical processes at surfaces and interfaces is a formidable challenge because a wide range of atomic environments and very different types of bonding can be present. In recent years interatomic potentials based on artificial neural networks (NNs) have emerged offering an unbiased approach to the construction of potential energy surfaces (PESs) for systems that are difficult to describe by conventional potentials. Here, we review the basic properties of NN potentials and describe their construction for materials like metals and oxides. The accuracy and efficiency are demonstrated using copper and zinc oxide as benchmark systems. First results for a potential of the combined ternary CuZnO system aiming at the description of oxide-supported copper clusters are reported.

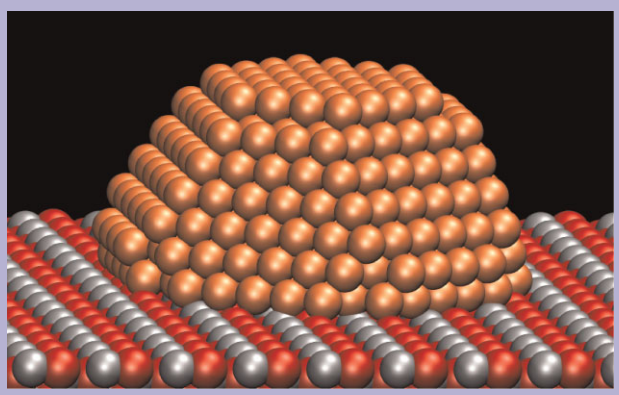

Model of a copper cluster at the ZnO($10\bar{1}0$) surface.

1 Introduction Supported metal clusters play an important role as catalysts for a number of large-scale processes in chemical industry, and in particular copper clusters supported at zinc oxide, which are used as catalyst for methanol synthesis from hydrogen and carbon monoxide [1], have received a lot of attention in recent years. Numerous experimental studies have provided valuable insights into their properties under various conditions [2–6]. Many interesting phenomena have been observed like copper zinc alloy formation under reducing conditions [7, 8], the oxidation of copper clusters at elevated temperatures [9], a strong interaction between the copper particles and the oxide support resulting in diffusion of copper atoms [10] or even clusters [11, 12] into the ZnO surface, and a reversible shape change of the clusters under varying gas phase conditions [13]. All these processes have a strong influence on the catalytic activity and must have consequences for the underlying reaction mechanisms. Therefore, a detailed understanding of the structural and dynamical properties of copper clusters at zinc oxide is an important step toward a deeper insight into the catalytic methanol synthesis.

Theoretical studies of large supported metal clusters could in principle provide important information to complement the experimental data, but they are severely hampered by the required system size as the copper clusters typically contain several thousand or even tens of thousands of atoms, and the zinc oxide support needs to be considered explicitly as well. Consequently, most theoretical studies on the mechanisms of methanol synthesis have been carried out for model systems addressing specific important details [14–16]. In particular density-functional theory (DFT) has been shown to be a useful tool to characterize the thermodynamic properties of the involved copper [17–19] and zinc oxide surfaces [20–22], and also a few studies on

small model systems of the combined system have been published [23, 24]. Still, many important aspects of the catalytic process like the role of large-scale defects and of complex atomic rearrangements as a function of temperature and the chemical composition of the system [13] cannot be studied directly by DFT, because the required systems are too large making the calculations computationally too demanding.

The construction of more efficient, but equally reliable interatomic potentials for large-scale simulations of complex systems, in particular for chemical processes at interfaces and in the field of materials science, is very challenging if several chemical elements are involved. Most of the established potentials are based on physically motivated approximate functional forms, *e.g.*, the Tersoff potential [25], embedded atom potentials [26, 27] and bond order potentials [28], and most potentials have been reported for elemental and binary systems only, while applications to multicomponent systems are very rare.

An alternative approach to the construction of efficient potentials is to use very flexible functions and to adjust these functions to reference data obtained in electronic structure calculations. Several methods have been suggested like genetic programming [29], polynomials [30], modified Shepard interpolation based on a Taylor expansion [31], interpolating moving least squares [32], Gaussian approximation potentials [33], or Kriging [34]. Also for these types of potentials the description of complex multicomponent systems is challenging, and compared to potentials based on physical approximations they are still much less frequently used.

Another method for constructing potentials employing very flexible functions is based on artificial neural networks (NNs). They have many properties making them interesting candidates for the construction of potential energy surfaces (PESs) [35, 36]. NNs have a rather simple functional form and can be calculated very efficiently. They are numerically accurate, allow for the making and breaking of bonds, and are equally applicable to all types of bonding irrespective of the physical nature of the interactions.

In the present work the properties and the construction of NN potentials for high-dimensional systems are reviewed with a focus on recent work on metals and oxides. Further, the applicability of this method to ternary systems is explored using supported copper clusters at zinc oxide as benchmark system. While NN potentials have been shown to work well for elemental and binary systems, to date high-dimensional NN potentials have not been applied to ternary systems including explicitly all degrees of freedom. A central question is if the overall accuracy is reduced due to the increased complexity of the ternary system or if potentials of a quality comparable to that of elemental and binary systems can be obtained. This will be tested not only by investigating the performance for the ternary system itself, but also by comparing the description of subsystems like metallic copper and zinc oxide with NN potentials constructed explicitly for these systems only.

2 Neural network potentials

Artificial NNs have first been developed to investigate the signal processing in the brain [37], but in recent decades they have also become a powerful tool for data analysis and pattern recognition with applications in many fields of science [38, 39]. Apart from these applications it has been shown that the class of feed-forward NNs can be used to approximate functions with in principle arbitrary precision, if a suitable set of function values is available for training the NN [40, 41]. This capability of NNs can be exploited in constructing PESs from a set of energy data obtained in electronic structure calculations. The resulting NN PESs are very efficient to calculate and can have a very high numerical accuracy [35, 36]. Analytic gradients for the calculation of interatomic forces required for instance for molecular dynamics (MD) simulations are readily available. In the last two decades NN potentials have been published for a wide range of small molecules [42–48] and also for the interaction of usually diatomic molecules with frozen metal surfaces [49–54], but the main limitation has been the restriction to small systems with only a few degrees of freedom.

Extensions of the NN method to construct PESs of high-dimensional systems are very rare, but they are mandatory for addressing many interesting chemical problems in materials and surface science. Apart from an early approach by Smith and coworkers [55, 56], which has been applied only to a few systems [57, 58], the most important generalization to large systems has been reported by Behler and Parrinello [59, 60]. In this method, which is used in the present work, the NN potential depends explicitly on the positions of all atoms and the construction of PESs for systems containing hundreds or even thousands of atoms is possible. In contrast to most conventional NN potentials the total energy is not expressed by a single NN, but for each atom in the molecule or solid an individual atomic NN is introduced. Each of these atomic NNs yields the energy contribution E_i of an atom i to the total energy E as a function of its local chemical environment. For a system containing M atoms the total energy is then given as

$$E = \sum_{i=1}^{M} E_i \,. \tag{1}$$

The resulting high-dimensional NN scheme is shown schematically in Fig. 1 for a system of composition $Cu_xZn_yO_z$. Each line corresponds to one atom in the system. Initially, only the Cartesian coordinate vectors $\boldsymbol{R}_i$ of the atoms are known, but they cannot be used directly as input for the atomic NNs. Instead, in a first step, the atomic positions are transformed to a vector of symmetry function values $\boldsymbol{G}_i$, which are many-body functions depending on the positions of all atoms in the chemical environment of atom i up to a cutoff radius. This cutoff needs to be increased until all relevant interactions are included and the NN PES converges to the desired accuracy. In the present work a cutoff radius of $R_c \approx 6.4$ Å is employed. The obtained symmetry function vectors can be viewed as structural

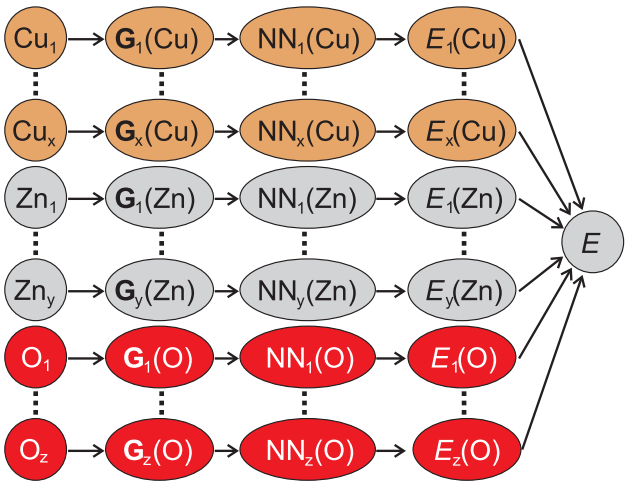

Figure 1 (online color at: www.pss-b.com) Schematic structure of a high-dimensional NN [59] for a system of the composition $Cu_xZn_yO_z$. For each atom i in the system there is one line. Each circle on the left side represents the Cartesian coordinate vector of an atom. These are then transformed to symmetry function vectors $\boldsymbol{G}_i$ describing the local atomic environments. The $\boldsymbol{G}_i$ are then used as input vectors for atomic NNs yielding the atomic energy contributions E_i to the total energy E.

fingerprints of the atomic environments and represent the input for the individual atomic NNs yielding the associated atomic energies. In the final step the contributions of all atoms in the system are added to obtain the total energy.

The symmetry functions describing the atomic environments need to have a number of properties to make them suitable input coordinates for the atomic NNs. First of all, the function values must be independent of rotation and translation of the system, because the energy of a system is only determined by the relative atomic positions. This excludes the direct use of Cartesian coordinates. Further, the number of symmetry functions must be independent of the number of neighboring atoms in the cutoff sphere. This is important, because the local coordination can change in MD simulations, while the number of input nodes of the NNs must remain fixed to ensure that all connecting weights are available. Finally, they need to be continuous in value and slope, since analytic derivative are needed for the calculation of atomic forces, but also for the application of gradient-based optimization algorithms used to determine the numerical values of the weight parameters.

In the present work two types of symmetry functions are used. Both types are many-body functions of all coordinates of all atoms inside the cutoff sphere, which is ensured by the cutoff function

$$f_c(R_{ij}) = \begin{cases} 0.5 \cdot \left[\cos\left(\frac{\pi R_{ij}}{R_c}\right) + 1\right] & \text{for} \quad R_{ij} \le R_c \\ 0 \quad \text{for} \quad R_{ij} > R_c, \end{cases} \tag{2}$$

of the distance R_{ij} between atom i and its neighbor j. It decays smoothly to zero in value and slope at the cutoff radius, and consequently all atoms j with $R_{ij} > R_c$ do not contribute.

The first type of symmetry function we use is the "radial function"

$$G_i^1 = \sum_{j \neq i} e^{-\eta R_{ij}^2} \cdot f_c(R_{ij}). \tag{3}$$

It consists of a sum of products of a Gaussian and the cutoff function. Using the Gaussian instead of the interatomic distance itself ensures that the symmetry function value decreases with increasing distance. This reflects the decaying atomic interaction with increasing separation. Multiplying the Gaussian by the cutoff function reduces the function value and its derivative exactly to zero at the cutoff radius. If the product of the Gaussian and the cutoff function would be used directly as symmetry function, there would be one symmetry function per neighboring atom. This would not allow to use these symmetry functions as input vector for an atomic NN, because the NN needs a constant number of input nodes for each possible atomic configuration. Therefore, according to Eq. (3) the products of all neighbors are added to yield a single number, which can be interpreted as a coordination number up to a certain distance from the central atom i. The spatial extension of the symmetry function can be controlled by the Gaussian parameter η. Reducing the cutoff itself is not a good choice because enforcing zero function values at short interatomic distance can cause strong oscillations in the derivatives [60].

The second type of symmetry function we use is the "angular function"

$$G_i^2 = 2^{1-\zeta} \sum_{j \neq i} \sum_{k \neq i,j} \left(1 + \lambda \cos\theta_{ijk}\right)^{\zeta} \cdot e^{-\eta\left(R_{ij}^2 + R_{ik}^2 + R_{jk}^2\right)} \cdot f_c(R_{ij}) \cdot f_c(R_{ik}) \cdot f_c(R_{jk}), \tag{4}$$

which describes the angular distribution of the neighboring atoms by summing the cosine terms of the angles $\theta_{ijk} = \arccos\left(\frac{\boldsymbol{R}_{ij} \cdot \boldsymbol{R}_{ik}}{R_{ij} \cdot R_{ik}}\right)$ centered at atom i. The parameter λ, which can have a value of $+1$ or -1, determines if the maximum of the cosine function is at $\theta_{ijk} = 0^\circ$ or at $\theta_{ijk} = 180^\circ$. The parameter ζ can be used to control the angular resolution, and typically a set of functions with different ζ values is used. Multiplying the cosine term by the cutoff functions of all three interatomic distances ensures that the contribution of the corresponding angle is zero if any of the distances in the triangle ijk is larger than the cutoff.

In general, we use a set of many radial and angular symmetry functions to describe the chemical environments of the atoms differing in the specific parameter values of η, ζ, and λ. These parameters are not optimized but determine the spatial resolution in the characterization of the atomic environments. In general we found that the obtained fitting accuracy is not very sensitive to the specific parameter set, and a given set of symmetry function values can typically be used for a wide range of materials.

For multicomponent systems like CuZnO the presence of different chemical species in the atomic environments

needs to be taken into account. For instance, an oxygen atom can have other oxygen atoms, zinc atoms, and copper atoms in its environment. Therefore, for each species a separate set of radial symmetry functions needs to be used. For the angular symmetry functions, there are six sets of functions corresponding to the respective pair combinations of the elements. This is shown on the left side of Fig. 2 for an atomic NN providing the energy of an atom of element X. In case of radial functions G^1 for each possible neighbor or in case of angular functions G^2 for each possible pair of neighbors there are N symmetry functions with different parameters, and N can be different for each group of symmetry functions. Further details about the symmetry functions can be found elsewhere [60].

Having established a suitable set of symmetry functions to describe the atomic environments, they are used as vectors of input values for the atomic NNs as shown schematically in Fig. 2. Each atomic NN consists of a number of nodes or neurons that are arranged in layers. The atomic NNs are basically standard feed-forward NNs, and their output values, the atomic energy contributions are calculated in the following way. First, the set of symmetry function values is provided in the nodes of the input layer on the left side. In Fig. 2 the symmetry functions are grouped according to the involved chemical species to illustrate the structure for the ternary CuZnO system. For the discussion we will not distinguish the different types of symmetry functions and use the general term G_j, and also in practical applications there is no difference in dealing with the symmetry functions of different groups of elements.

The input nodes are connected to the nodes in the first hidden layer by so-called weight parameters, and here we use the symbol a_{ij}^{kl} for the connection between node i in layer k and node j in layer $l = k + 1$. The weight parameters are the fitting parameters of the NN. The values y_j^l of node j in layer l are then calculated as a linear combination of the symmetry function values at the input nodes using the weight parameters as coefficients. Further, at each node a bias weight b_j^l is added, which is used as an adjustable offset to shift the non-linear part of the activation function f, which is finally applied. A wide range of functions can be used as activation functions, and here we use the hyperbolic tangent. The purpose of the activation functions is to provide the functional flexibility needed to represent complicated PESs with high accuracy. Finally, at each node of the first hidden layer a single number is obtained.

In the next step, the values of the nodes in the second hidden layer are calculated in the same way and so on until the output value is obtained. The full analytic form of the example NN shown in Fig. 2 is then given by

$$E_i = f_1^3\left(b_1^3 + \sum_{l=1}^{10} a_{l1}^{23} \cdot f_l^2\left(b_l^2 + \sum_{k=1}^{10} a_{kl}^{12} \cdot f_k^1\left(b_k^1 + \sum_{j=1}^{N_{\mathrm{tot}}} a_{jk}^{01} \cdot G_j\right)\right)\right). \tag{5}$$

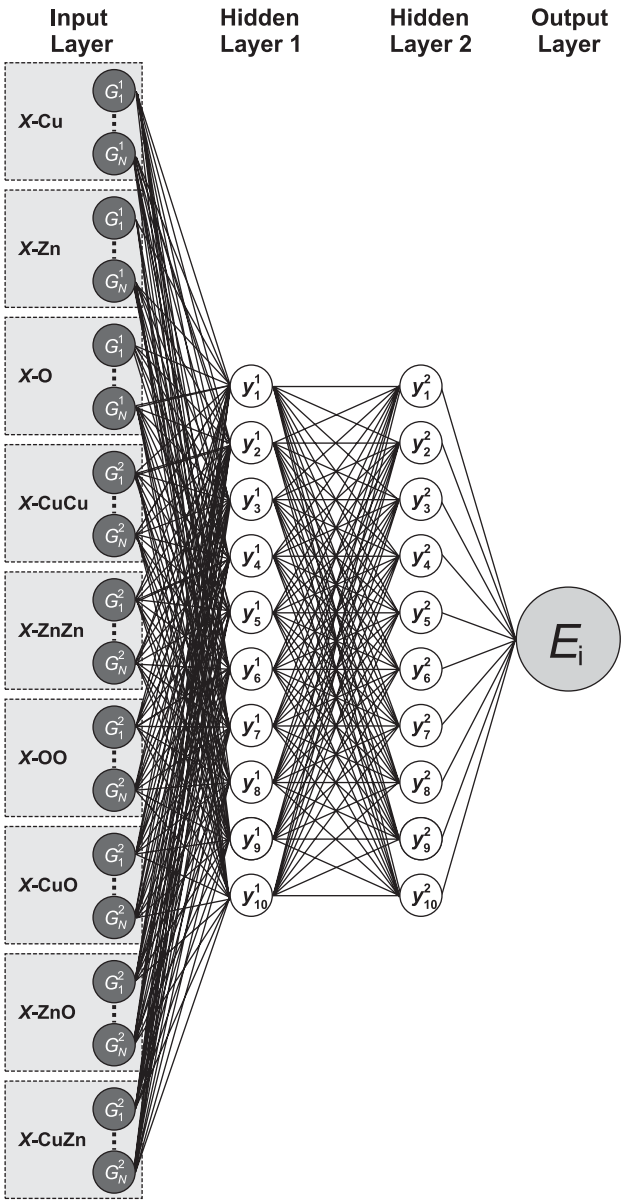

Figure 2 Structure of an atomic NN for element $X = (\mathrm{Cu}, \mathrm{Zn}, \mathrm{O})$ in the ternary CuZnO system. In this example the NN consists of two hidden layers, and each hidden layer contains ten nodes. Node j in layer k has the value y_j^k, and all nodes in adjacent layers are connected by weight parameters shown as black lines. The input vector $\boldsymbol{G}_i$ of symmetry function values contains groups of radial symmetry functions G^1 specified by one neighboring element and angular symmetry functions G^2 defined by two neighboring elements. The numbers N of symmetry functions in each group represented by the dashed boxes can vary. The atomic energy contribution E_i is the weighted sum of the node values in the second hidden layer. The complete functional form of the atomic NN is given in Eq. (5). For clarity the bias weight connections are not shown.

The number of hidden layers and the number of nodes per layer, *i.e.*, the architecture of the NN, can be described by a short hand notation. According to this notation the NN in Fig. 2 is an N_{tot}-10-10-1 NN, with N_{tot} being the total

number of symmetry functions. Different architectures can be used for different elements in the system, but for a given element the architecture must be the same for all atoms.

The accuracy of the obtained total energies depends on the numerical values of the weight parameters of the atomic NNs. They are determined in an iterative optimization process employing a known set of reference energies from electronic structure calculations for representative atomic configurations. The atomic NNs in Fig. 1 all have the same structure and weight parameter values for a given element, and consequently three sets of weight parameters need to be determined. They are not independent since there is only one total energy per structure. Therefore, they are optimized simultaneously using the total energy as the target quantity. Once a reliable set of weight parameters has been found that reproduces the training set with the desired accuracy, the weight parameter values are frozen and the NN can be used in applications. The systems can then be of arbitrary size, because if an atom is added, the high-dimensional NN scheme is extended by another atomic NN for the respective element, while if an atom is deleted, its atomic NN is removed. Further details on the method can be found elsewhere [59, 60].

NN potentials have well-defined functional forms and therefore analytic gradients can be calculated which provide access to the atomic forces. The force $F_{i,\alpha}$ acting on atom i in direction $\alpha = \{x, y, z\}$ is given as the partial derivative of the total energy with respect to the Cartesian coordinate $R_{i,\alpha}$. In the explicit evaluation of the forces the transformation onto symmetry functions has to be taken into account as

$$\begin{aligned} F_{i,\alpha} &= -\frac{\partial E}{\partial R_{i,\alpha}} \\ &= -\sum_{k=1}^{M} \frac{\partial E_k}{\partial R_{i,\alpha}} \\ &= -\sum_{k=1}^{M} \sum_{j=1}^{N_k} \frac{\partial E_k}{\partial G_{k,j}} \frac{\partial G_{k,j}}{\partial R_{i,\alpha}}. \end{aligned} \tag{6}$$

The partial derivatives $\partial G_{k,j}/\partial R_{i,\alpha}$ are given by the definition of the employed symmetry functions, and the terms $\partial E_k/\partial G_{k,j}$ are defined by the architecture of the NN and the weight parameters. It should be noted that although the atomic energy contributions depend on the local chemical environment inside the cutoff spheres, the atomic forces depend also on atoms within a distance of up to twice the cutoff radius. The reason is the construction of the total energy as a sum of individual atomic energies, which in turn depend on many-body symmetry functions. The force $F_{i,\alpha}$ is the sum of all atomic energy derivatives with respect to $R_{i,\alpha}$ and consequently all atoms k having atom i in their environment enter the force. However, the atomic energy contributions simultaneously depend also on the positions of all other atoms via the symmetry functions. Therefore, the dependence of the forces on the atomic positions has a maximum range of twice the cutoff radius, which is fully consistent with the total energy expression of the NN.

NN potentials of the Behler Parrinello scheme have been successfully constructed for a number of materials like silicon [61, 62], sodium [63, 64], carbon [65, 66], copper [67, 68], and the phase change material GeTe [69–71]. The accuracy can be further improved by taking long-range electrostatic interactions into account explicitly, which are not truncated at the cutoff radius. It has first been proposed by Popelier and coworkers to employ NNs to construct environment-dependent atomic charges [72]. The first NN total energy surfaces employing environment-dependent atomic charges have been constructed for zinc oxide [73] and for the water dimer [74] as an extension of the Behler Parrinello method described above. Although very accurate PESs have been obtained for these systems, a large fraction of the electrostatic interactions can also be captured by atomic energy contributions only depending on the local chemical environment, because they are able to cover all atomic interactions up to the cutoff radius irrespective of their physical nature. Including electrostatic interactions explicitly using environment-dependent charges increases the computational costs of the NN energy evaluation because a second set of atomic NNs needs to be introduced to derive the atomic charges [73], and an Ewald summation has to be used to obtain the electrostatic energies and forces. Therefore, in the present work we explore if a high-quality potential for the ternary CuZnO system can be obtained following a generalized multicomponent version of the high-dimensional NN method suggested by Behler and Parrinello [59].

3 Computational details The NN potential for the ternary CuZnO system has been constructed using DFT as reference method as implemented in the all-electron code FHI-aims [75]. The Kohn–Sham orbitals are expanded in a basis of atom-centered numerical atomic orbitals (“second tier” basis for oxygen, “first tier” basis for copper and zinc), which allows to carry out calculations with and without periodic boundary conditions in a numerically consistent way. For periodic systems, converged k-point grids have been used with a k-point density corresponding to a $12 \times 12 \times 12$ grid for the four-atom unit cell of fcc copper. The PBE functional has been selected to describe electronic exchange and correlation [76].

Based on this reference data, the NN potential has been constructed using our NN code RuNNer [77]. For this purpose, the reference set is split into a training set, which is used to optimize the weight parameters of the atomic NNs, and an independent test set to check the quality of the potential for structures not included in the training set. A low root mean squared error (RMSE) of the test set energies and forces indicates that no significant overfitting, *i.e.*, a poor description of structures in between the training points, is present and that the potential is sufficiently transferable. For the optimization of the weight parameters a wide range of standard optimization algorithms can be used. Here, we employ the adaptive global extended Kalman filter [78]. In

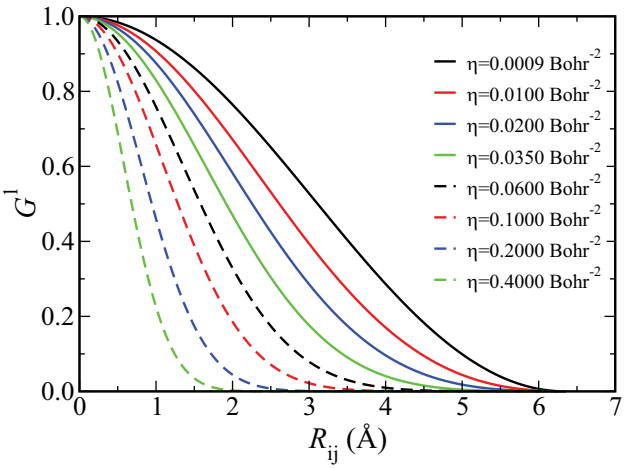

Figure 3 (online color at: www.pss-b.com) Radial symmetry functions used in the NN potential for the ternary CuZnO system [60]. The plots show only the product of the Gaussian and the cutoff function, the summation in Eq. (3) is not included for clarity. The same set of functions is used to describe the radial environment of each atom, and for each possible neighboring element an identical set of functions is used.

addition to the total energies also the DFT forces, which provide a large amount of information on the shape of the PES, are used to find the optimum set of weights.

The functional flexibility of the NN potential is determined by the architectures of the atomic NNs. The larger the NNs, the more fitting parameters are available. If this number is too large, overfitting may occur. If it is too small, the NN cannot adjust to the training data and poor potentials will be obtained. Therefore, we generally construct a number of potentials employing different numbers of hidden layers and nodes per layer to determine the optimum NN architecture. The input vector for the atomic NNs is given by a set of symmetry functions describing the atomic environments. In the present work we use 156 symmetry functions for each element. They include a set of eight radial functions [*cf.* Eq. (3)] employing different Gaussian exponents for each of the three possible neighboring elements, yielding in total 24 radial symmetry functions for each atom. The set of radial functions is plotted in Fig. 3 for an arbitrary neighboring element. Further, 132 angular functions are used [*cf.* Eq. (4)]. The parameters defining all employed symmetry functions are given in the Supporting Information [79].

4 Results and discussion

4.1 Construction of the neural network potential energy surface for CuZnO The reference dataset for constructing the NN potential for the ternary CuZnO system includes the DFT energies of about 100 000 structures comprising clusters, bulk structures and slabs with up to about 100 atoms. It contains the copper data [67] and zinc oxide data [73] used in earlier work to construct NN potentials for these subsystems, as well as new data for the ternary system and some configurations of the binary CuZn and CuO systems. Apart from a reliable description of the copper clusters and the zinc oxide support, we are primarily interested in obtaining an accurate NN potential for the interface between the copper clusters and the zinc oxide. Therefore, we do not aim to obtain a potential that will be valid also for chemically very different systems like molecular O_2 or metallic zinc. Consequently, no structures for these systems are included.

In general, the reference configurations contain ideal and distorted bulk structures and slabs, but also snapshots from MD simulations at different temperatures and pressures. Additionally, a large number of clusters is included. Further details of the protocol used for generating the training set in a systematic way have been described elsewhere [67]. In essence, we iteratively refine the potential and suggest new configurations for DFT calculations by running MD simulations employing energies and forces obtained from preliminary NN potentials. For each fit, the reference dataset has been split into a training set containing about 90% of the data points, and an independent test set to check the accuracy. The compositions of the finally obtained training set and test set are compiled in Table 1.

Several NN architectures have been tested to find the optimum NN to represent the PES of the CuZnO system. Our goal is to avoid system-specific modifications of the NNs, and consequently the same architecture has been used for all three types of atomic NNs yielding the energy contributions of the copper, zinc, and oxygen atoms, respectively. Also the same set of symmetry functions has been used for simplicity to describe the chemical environments of the atoms, although a more sophisticated element-specific selection of the symmetry functions might reduce their number. The results for the RMSEs of the energies and forces are listed in Table 2. The best fit, which is shown in bold in the table, contains three hidden layers and 15 nodes per layer. It has been selected because it has the smallest error for the energies in the test set and also the lowest RMSEs for the forces. The RMSE values of the energies in the training and the test set are 4.8 and 5.1 meV atom^{-1}, respectively, the RMSEs of the training and test set forces are about 94 and 89 meV Bohr^{-1}. The very similar values for the training set and the test set indicate that basically no overfitting is present and that in the configuration space determined by the reference data unknown structures are well described. In

Table 1 Composition of the training set and the test set.

system	training set			test set		
	clusters	bulk	slabs	clusters	bulk	slabs
Cu	5810	10,604	12,484	670	1125	1405
ZnO	7105	24,572	3695	833	2715	402
CuZn	4	588	1122	–	61	128
CuO	37	909	–	5	106	–
CuZnO	18,356	–	2317	2033	–	263

Table 2 RMSEs of the NN energies and forces obtained for the training set and the test set of the ternary CuZnO system with different NN architectures. The fit used in the present work is shown in bold. Further, the number of weight parameters in the atomic NNs is given for each architecture.

network architecture	weights per element	E_{RMSE} (meV atom^{-1})		F_{RMSE} (meV Bohr^{-1})	
		training set	test set	training set	test set
156-2-2-1	323	8.129	8.215	137.2	133.3
156-2-2-2-1	329	8.666	8.729	134.6	131.5
156-5-5-1	821	5.884	6.195	112.2	110.9
156-5-5-5-1	851	5.539	5.908	102.8	100.2
156-10-10-1	1691	5.322	5.683	99.0	95.1
156-10-10-10-1	1801	4.991	5.360	95.6	93.1
156-15-15-1	2611	5.285	5.638	99.2	96.7
156-15-15-15-1	**2851**	**4.844**	**5.132**	**93.1**	**88.6**
156-20-20-1	3581	5.905	6.233	109.1	105.2
156-20-20-20-1	4001	5.351	5.682	99.2	95.3
156-30-30-1	5671	7.114	7.349	117.4	112.6
156-40-40-1	7961	8.913	8.907	139.0	133.4

total the NN potential contains 2851 weight parameters for each of the three elements, which have been determined using approximately 8,000,000 pieces of information from the DFT total energies and force components.

In the following sections, the properties of this NN potential are studied in detail. First, the two subsystems copper and zinc oxide are discussed separately, and the results are compared to the properties of NN potentials previously constructed specifically for these systems. Since constructing a potential for the ternary system is substantially more challenging than for a pure metal or a binary oxide, it is of high interest to investigate if the accuracy is comparable to that of NN potentials customized for these subsystems or if the accuracy decays with the number of elements in the system because of the increasing complexity of the configuration space. Then, first preliminary results are presented for the ternary CuZnO system. In particular, the quality of the potential at the interface between a large copper cluster and a zinc oxide support is investigated.

4.2 Neural network potential for copper The first system we study is pure copper. For this system an NN potential-based essentially on the same copper structures as used for constructing the ternary NN PES has been published previously [67]. In Table 3 bulk properties like the lattice parameters, cohesive energies and bulk moduli for several crystal structures obtained with both NN PESs are listed and compared to the corresponding DFT values. For all structures both NN potentials yield basically the same results with only very small deviations from the DFT data.

Next, we have investigated the surface energies of relaxed clean low-index copper surfaces, which are important benchmarks for a reliable description of very large copper clusters exhibiting a number of facets. They are compiled in Table 4. Like for bulk copper, the agreement between the two NN potentials and DFT is excellent and fitting the more complex ternary system does not reduce the

Table 3 Comparison of the lattice parameters, cohesive energies, and bulk moduli of various crystal structures of copper obtained with two NN potentials and DFT.

property	NN	NN	DFT
	this work	for Cu [67]	
fcc structure			
a_0 (Å)	3.628	3.630	3.630
E_{coh} (eV)	3.524	3.526	3.533
B (GPa)	142	138	140
bcc structure			
a_0 (Å)	2.885	2.887	2.885
E_{coh} (eV)	3.492	3.486	3.489
B (GPa)	139	135	137
simple cubic structure			
a_0 (Å)	2.407	2.407	2.407
E_{coh} (eV)	3.051	3.052	3.051
B (GPa)	100	108	103
hcp structure			
a_0 (Å)	2.568	2.570	2.573
c/a_0	1.629	1.631	1.627
E_{coh} (eV)	3.525	3.511	3.511

Table 4 Surface energies of low index copper surfaces obtained from DFT and the NN potential for the ternary CuZnO system. For comparison also the NN surface energies obtained from a potential for pure copper [67] are listed. All energies are given in meV Å^{-2}, "mr" is the missing row reconstruction.

surface	NN	NN	DFT
	this work	for Cu [67]	
(100)	98.3	101.0	100.5
(110)	102.6	103.9	102.4
(110)mr	109.8	111.7	109.9
(111)	88.7	92.7	93.2

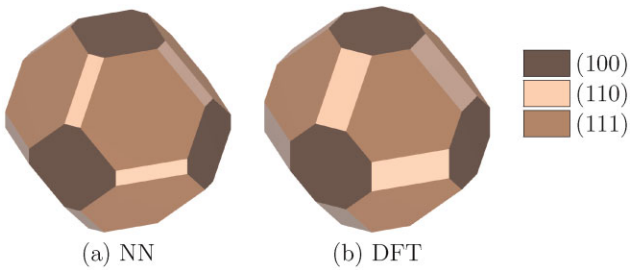

Figure 4 (online color at: www.pss-b.com) Wulff constructions [80] for copper clusters obtained from the NN potential of the ternary CuZnO system and from DFT.

accuracy of the description of pure copper. Based on these surface energies, we have determined the equilibrium shapes of free copper clusters using a Wulff construction [80, 81]. The resulting clusters are illustrated in Fig. 4 showing that the NN potential and DFT predict very similar shapes for very large ideal clusters.

Copper clusters used in heterogeneous catalysis are far from these ideal conditions and defects will play an important role. We have thus constructed a model for the Cu(111) surface containing about 19,000 atoms including a step and a large terrace with several imperfections like kinks, adatoms, and vacancies (Fig. 5). We note that this surface structure has been built employing interatomic distances of bulk copper and has not been relaxed to provide sizeable forces acting on the atoms for further analysis. While the NN potential is very efficient and allows to calculate the energy of this model system in a few seconds, this is not possible for DFT due to the large system size. Consequently, instead of total energies we have used the atomic forces as local probes for the shape of the PES. For this purpose, we have selected ten representative atoms shown in blue in Fig. 5. As discussed above, the NN forces acting on these atoms depend on all neighboring atoms with a distance up to twice the cutoff radius of the symmetry functions used to describe the local chemical environments of the atoms. Therefore, we have cut clusters centered at these atoms that we use to calculate the DFT forces at the central atoms. These clusters are shown in Fig. 6 and also as transparent blue spheres in Fig. 5. They contain on average about 260 atoms and are sufficiently large to ensure that the central atoms have approximately the same chemical environment as in the full system. In Fig. 7 the DFT forces obtained in the cluster calculations are compared to the corresponding NN forces of the ternary potential in the slab. By construction the NN forces in the full slab are the same as the NN forces in the large clusters. In general, the agreement is excellent, and only for one cluster there is a deviation of about 0.1 eV Bohr^{-1}.

4.3 Neural network potential for zinc oxide

The second important subsystem is zinc oxide, which is frequently used as support oxide in heterogeneous catalysis. In Table 5 the lattice parameters, cohesive energies, and bulk moduli of several crystal structures of ZnO are compared for the ternary CuZnO NN potential of the present work, an NN

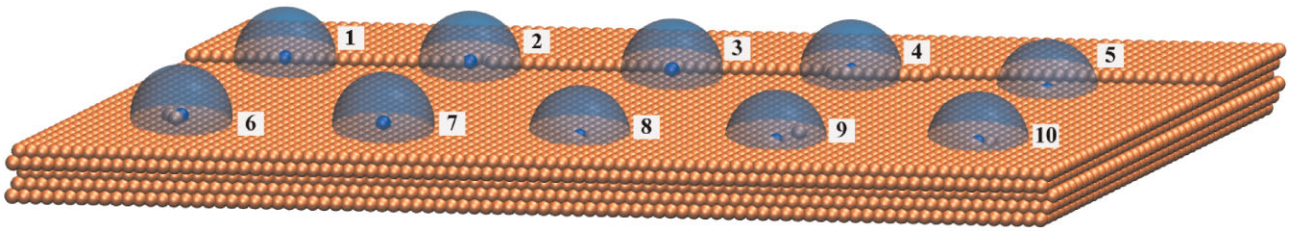

Figure 5 (online color at: www.pss-b.com) Slab model of a Cu(111) surface with several defects like vacancies, adatoms, steps, and kinks. Ten representative atoms shown in blue have been selected to investigate the accuracy of the NN PES. The NN forces acting on these atoms depend on all atoms inside the transparent spheres with a radius of approximately 12 Å, which corresponds to twice the cutoff R_c of the symmetry functions. The atoms enclosed in these spheres form clusters which are small enough to be calculated by DFT. They are shown in Fig. 6.

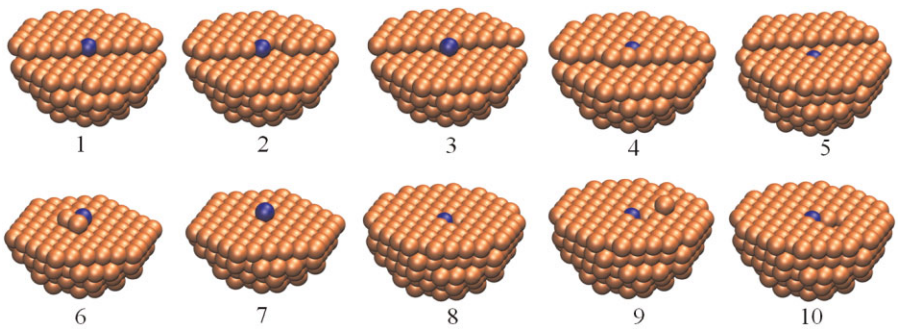

Figure 6 (online color at: www.pss-b.com) Structures of the ten clusters extracted from the large slab model of the Cu(111) surface in Fig. 5. The forces acting on the central atoms shown in blue can be used to assess the accuracy of the NN potential for the full system. A comparison of the DFT forces in these clusters and the NN forces in the full slab is shown in Fig. 7.

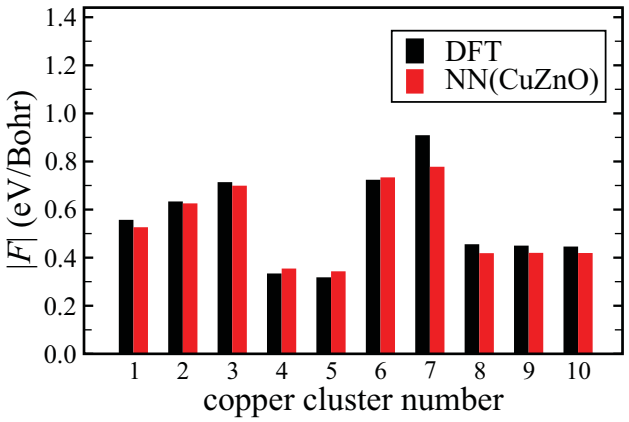

Figure 7 (online color at: www.pss-b.com) Comparison of the DFT and NN forces acting on the central atoms of the ten clusters shown in Fig. 6. The clusters used for the DFT calculations contain all atoms within a radius of about 12 Å around the central atom. By construction the NN forces in these clusters are identical to the NN forces in the full slab shown in Fig. 5.

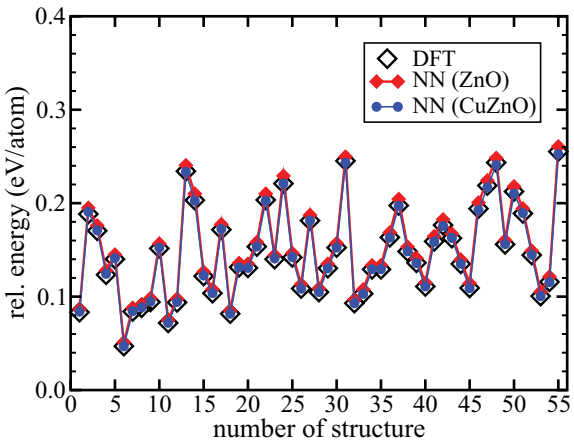

Figure 8 (online color at: www.pss-b.com) Comparison of the DFT and NN energies of random bulk structures of the composition Zn_4O_4. The NN energies have been obtained using two different potentials, a previously published NN potential for zinc oxide [73] (red diamonds) and the NN potential for the ternary CuZnO system of the present work (blue circles).

potential for pure ZnO reported previously [73] and DFT. The ZnO structures included in the underlying training sets of both NN potentials contain about 35,000 atomic configurations. We find very similar results and like in the case of pure copper the NN PES for the ternary system is of the same quality as the potential constructed for pure ZnO, which shows that the NN is sufficiently flexible to adapt to the complexity of the ternary system without loss in accuracy.

Further, in Fig. 8 the energies of a set of random ZnO bulk structures of composition Zn_4O_4 are plotted for both NN potentials and DFT to illustrate the performance for non-crystalline, amorphous structures. For these structures, it can be seen that the NN PES for the ternary system is even slightly superior to the original NN PES for ZnO. This provides confidence that neglecting long-range electrostatic interactions acting beyond the cutoff radius of the symmetry functions does not give rise to a significant error in the NN PES of the ternary system.

Apart from total energies we have also compared the forces acting on the atoms. In Fig. 9 the forces acting on the oxygen and zinc atoms of a $Zn_{15}O_{15}$ cluster extracted randomly from an MD simulation at 1000 K are shown. Like the bulk structures in Fig. 8 also this cluster has not been

Table 5 Comparison of the lattice parameters, bulk moduli, and cohesive energies per formula unit of several crystal structures of ZnO obtained with two NN potentials and DFT.

property	NN	NN	DFT
	this work	for ZnO [73]	
CsCl structure			
a_0 (Å)	2.692	2.680	2.688
E_{coh} (eV)	5.584	5.588	5.584
B (GPa)	156	160	159
NaCl structure			
a_0 (Å)	4.332	4.344	4.328
E_{coh} (eV)	6.751	6.745	6.747
B (GPa)	167	169	165
zincblende structure			
a_0 (Å)	4.624	4.612	4.616
E_{coh} (eV)	7.042	7.041	7.043
B (GPa)	125	133	129
wurtzite structure			
a_0 (Å)	3.278	3.278	3.278
c/a_0	1.614	1.614	1.614
u	0.379	0.379	0.379
E_{coh} (eV)	7.062	7.054	7.057

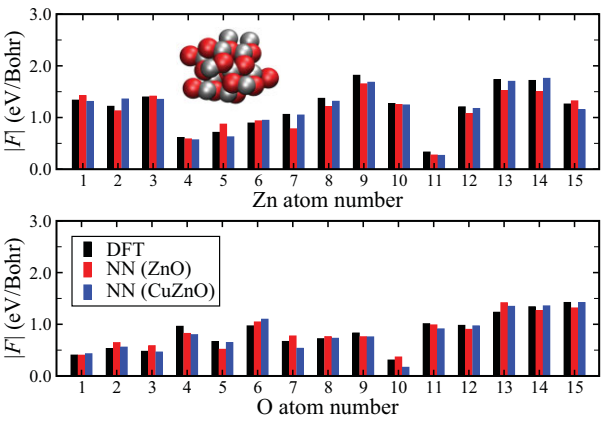

Figure 9 (online color at: www.pss-b.com) Comparison of the absolute forces acting on the atoms in a $Zn_{15}O_{15}$ cluster obtained by DFT and two NN potentials. The cluster has been chosen randomly from an MD simulation at 1000 K. The NN forces have been obtained using two different potentials, a previously published NN potential for zinc oxide [73] (red bars) and the NN potential for the ternary CuZnO system of the present work (blue bars).

included in the training set of the NN. Nevertheless, the agreement with the corresponding DFT forces is excellent.

4.4 Neural network potential for copper clusters at zinc oxide Constructing an NN potential for the ternary CuZnO system is very challenging because of the large configuration space. Here, we restrict ourselves to the construction of a potential suitable for describing the interaction between a copper cluster and a zinc oxide surface. The potential should be applicable to MD simulations of very large systems containing ten thousands of atoms to allow for studying clusters of a size comparable to experiment. Although some of the possible subsystems like metallic zinc are not relevant for these studies, the potential still needs to be reliable for many subsystems as different as large copper particles, zinc oxide, a variety of surfaces of both systems and their interfaces including a manifold of defects. All these subsystems need to be described accurately at different temperatures to ensure that MD simulations yield reliable results for varying conditions. Further, complex chemical processes can in principle take place at the interface resulting in structures strongly differing from the combination of the ideal subsystems. Diffusion of oxygen and zinc atoms into the copper cluster can give rise to the oxidation of the cluster and to alloy formation, respectively. On the other hand there is experimental evidence that copper clusters penetrate the ZnO surface giving rise to substantial structural changes in the ZnO support including significant mass transport [11].

It is very difficult to predict which structures are required in the training set to cover all relevant configurations. If important structures are missing, the NN potential is likely to fail because it has only very limited extrapolation capabilities. Nevertheless, it is very easy to detect such situations, and this can be used to improve the NN potential step by step by running MD simulations to generate many trial configurations, which are then searched systematically for important structures missing in the reference data. A straightforward possibility to detect structures resulting in extrapolation is to compare the symmetry function values of a given structure with the range of values of the symmetry functions in the training set. If a symmetry function is outside the interval spanned by the training data, the structure should be added to the training set. Another possibility, which also allows to detect "holes" in the training set is to construct several fits using the same training data. Due to the large flexibility of NNs these fits will provide similar energies and forces only for configurations sufficiently close to the training points. For structures far away, the NNs will differ strongly. This can be identified by comparing the energy and force predictions of several NN potentials for the trial structures. If a deviation is too large, a DFT calculation should be carried out and the point should be added to the training set. This approach is very efficient since DFT calculations need to be carried out only for structures that are missing. Since the atomic energy contributions only depend on the atoms in the local chemical environment, it is not necessary to perform DFT calculations for the full systems. Instead, if an atomic environment is missing, a cluster with the cutoff radius of the symmetry functions can be cut from the system, and a DFT calculation for this cluster can provide the required information for improving the NN. This allows to employ very large and realistic systems representative for the intended large-scale applications to improve the training sets. In Fig. 10 the NN and DFT energies of some examples for such clusters of the composition $Cu_{53}Zn_{10}O_9$, which have been cut from very large interface systems, are compared after refining the NN potential using these clusters. As can be clearly seen, the NN potential is able to reproduce the energies very well.

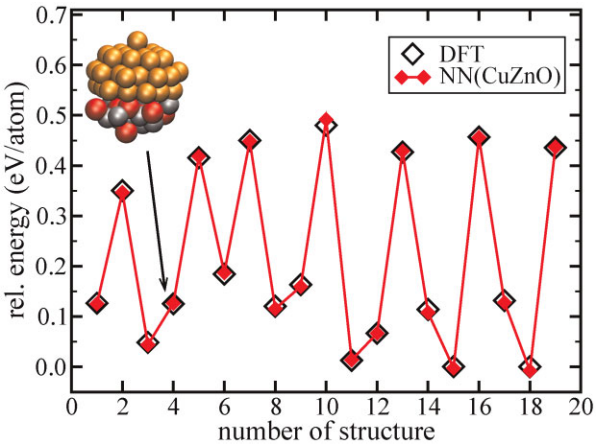

Figure 10 (online color at: www.pss-b.com) Comparison of the DFT and NN energies of clusters of the composition $Cu_{53}Zn_{10}O_9$.

Following this approach a first preliminary NN potential for the description of the interface between copper and zinc oxide has been constructed. As a first test we use a copper cluster containing 612 atoms, which is adsorbed with its (111) facet at a ZnO($10\bar{1}0$) surface. In total the system contains 7524 atoms. Initially, the structure of the system has been optimized using the NN potential. Then using the program TINKER [82], an *NVT* MD simulation at 1000 K has been carried out to obtain highly distorted structures at the interface. Like for the copper slab discussed in Section 4.2 the system is too large to carry out DFT calculations. Instead, we have selected representative atoms close to the interface to check the reliability of the NN potential using the atomic forces. Other atoms far away from the interface are embedded in chemical environments similar to pure copper or pure zinc oxide, which are accurately described as shown above. In Fig. 11(b) a snapshot of the MD simulation is shown. For a visualization of the interface the bottom side of the copper cluster is shown in panel (a), while a top view of the ZnO surface is shown in (c) including information about the positions of the copper atoms in the first layer in the cluster. Five atoms of each element have been selected as labeled in Fig. 11(a) and (c). Clusters centered at these atoms have been cut from the full system to determine the forces by DFT calculations. Using a radius of about 12 Å,

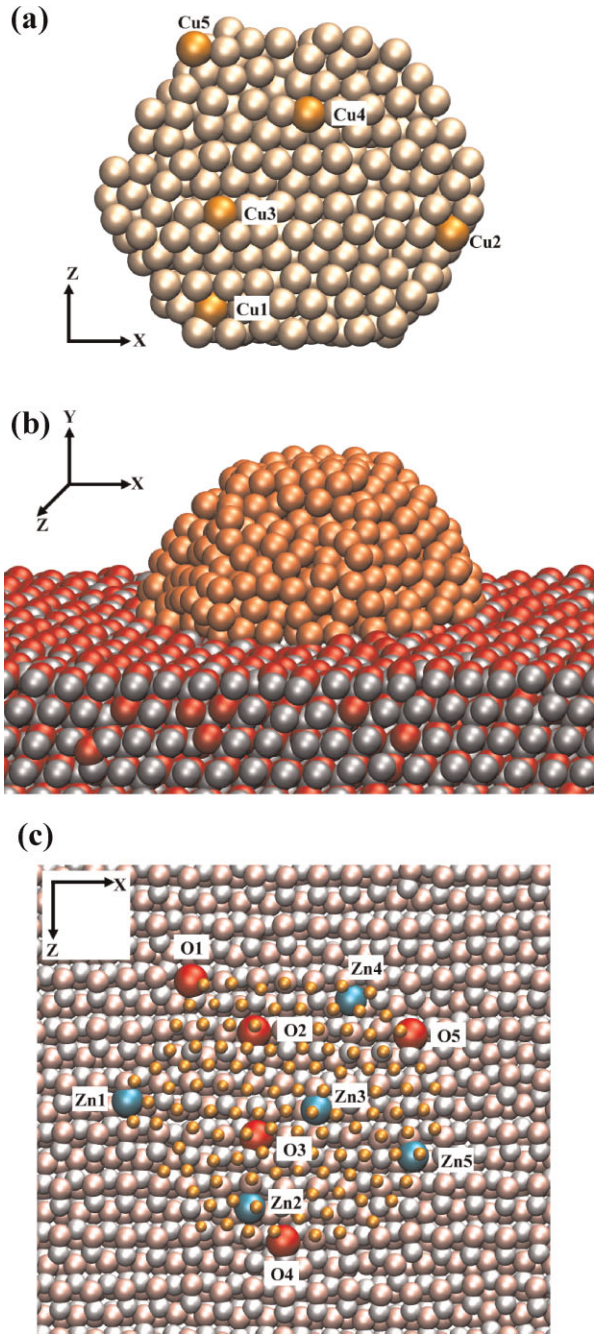

Figure 11 (online color at: www.pss-b.com) Snapshot of an MD simulation at 1000 K of a Cu_{612} cluster at the ZnO(10$\bar{1}$0) surface (b). This structure has been used to analyze the quality of the NN potential for the description of the interface atoms. In (a) a bottom-view of the cluster is shown and five copper atoms have been selected to compare the NN forces with the DFT forces. The comparison is shown in Fig. 12. In panel (c) a top view of the ZnO(10$\bar{1}$0) surface is shown. Five oxygen and five zinc atoms have been chosen for a closer investigation of the forces. In order to illustrate the position of these atoms with respect to the copper cluster, the copper atoms of the first metal layer, which are directly in contact with the ZnO surface, are shown as small spheres.

which corresponds to twice the cutoff radius of the symmetry functions, results in an average of about 450 atoms per cluster, which is still too large for DFT. We have therefore reduced the radii of the clusters for the DFT calculations to 6 and 9 Å corresponding to average numbers of 65 and 200 atoms, respectively. Using these two different cluster sizes allows to determine the level of convergence of the DFT forces acting on the central atoms as a function of the radius of the clusters. The results are plotted in Fig. 12. There are only small differences in the DFT forces at the central atoms in the 6 and 9 Å clusters, and both datasets are very similar to the NN forces calculated for these atoms in the full slab shown in Fig. 11. There are basically no differences in the quality of the NN forces for the elements copper, zinc, and oxygen. Since the DFT forces are converged already at cluster radii of 9 Å, we have also analyzed the effective convergence of the NN forces as a function of the cluster radius in Fig. 13. While in principle the NN forces depend on the positions of the atoms up to twice the cutoff radius away from the central atom, in practice the influence of distant atoms is very small, and it can be seen that for all atoms even the forces in the smallest clusters are already a very good approximation to the converged forces.

5 Conclusions and outlook The construction of high-dimensional NN potentials for multi-component systems has been reviewed. In general, NN potentials are very accurate and can provide PESs numerically close to the underlying reference electronic structure calculations, while the efficiency is several orders of magnitude higher. Compared to other potentials the construction of NN potentials is computationally more demanding due to the large number of training points required, but this effort is quickly regained in large-scale applications of the NN to systems, which are not accessible by electronic structure calculations.

Preliminary results for a DFT-based NN potential for the ternary CuZnO system have been reported. First, the accuracy for important subsystems like copper or zinc oxide, which are also of interest on their own, is investigated and compared to data obtained from previously published NN potentials for the individual subsystems. We found that the NN potential for the ternary system is of at least comparable quality for these subsystems although in principle fitting all training data for the ternary system is significantly more challenging. This clearly shows that NN potentials are able to represent complex PESs of multi-component systems and that their limit has not been reached by the potentials constructed to date for elemental and binary systems. For the ternary system first promising results have been obtained using a copper cluster at a ZnO support as benchmark system. The forces at the interface atoms have a quality comparable to that of the atoms in the simpler pure copper and zinc oxide subsystems. Still, the NN PES for the ternary CuZnO system is not yet expected to work equally well for all applications and further improvement of the potential is currently in progress. The present results demonstrate that NN potentials

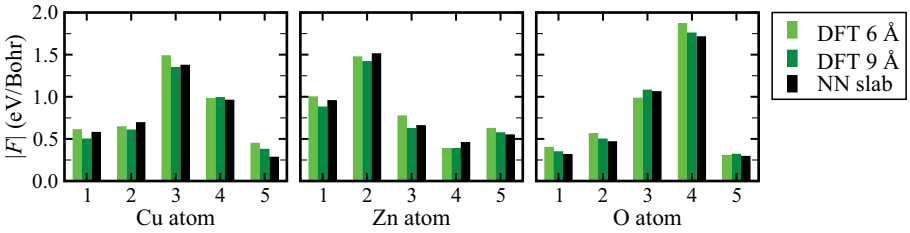

Figure 12 (online color at: www.pss-b.com) Comparison of the NN forces acting on selected atoms at the Cu(111)/ZnO(10$\bar{1}$0) interface shown in Fig. 11 and forces obtained by DFT in calculations for clusters centered at these atoms with radii of 6 and 9 Å.

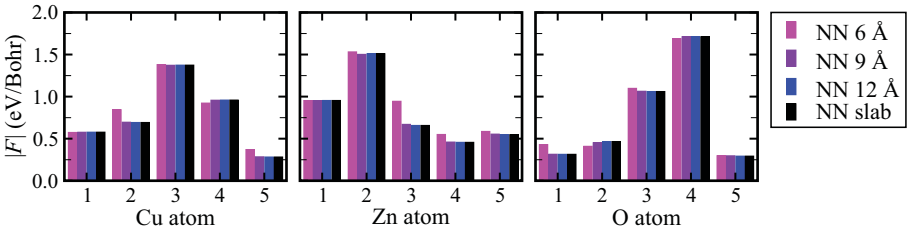

Figure 13 (online color at: www.pss-b.com) Convergence of the NN forces acting on selected atoms at the Cu(111)/ZnO(10$\bar{1}$0) interface shown in Fig. 11. The forces have been obtained from clusters centered at these atoms with increasing radii of 6, 9, and 12 Å. For comparison also the forces obtained directly for the full system are shown ("slab"). While there are still small differences between the 6 Å clusters and the slab, the forces are well converged for a cluster radius of 9 Å.

offer an interesting approach to construct PESs for a variety of complex materials and interfaces.

Still, there are also open challenges for the NN method. The number of elements that can be included is currently limited to about four for practical reasons because the number of symmetry functions used to describe the chemical environments of the atoms grows rapidly with the number of chemical species. This would allow to include hydrogen in the present potential, which is certainly also important for describing the cluster shape under catalytic conditions. However, a comprehensive study of the elementary steps of the catalytic methanol synthesis would further require to include carbon as a fifth species, which is presently beyond the scope of our approach. Further methodical developments to overcome this limitation are currently in progress. An alternative way to study the individual reaction steps would be to use an embedding scheme describing the majority of the cluster and the oxide support by an NN potential and the active site directly by DFT. The high accuracy and numerical consistency of the NN energies and forces with DFT might be a significant advantage for such an approach.

Acknowledgements We thank the DFG (SFB 558, Emmy Noether program) for financial support. Discussions with the FHI-aims team and computing time provided by the Ressourcenverbund NRW and LiDOng are gratefully acknowledged.

References

[1] J. B. Hansen, in: "Handbook of Heterogeneous Catalysis", edited by G. Ertl, H. Knötzinger, and J. Weitkamp (Wiley-VCH, Weinheim, 1997).
[2] J. D. Grunwaldt, A. M. Molenbroek, N.-Y. Topsøe, H. Topsøe, and B. S. Clausen, J. Catal. **194**, 452 (2000).
[3] M. Behrens, F. Studt, I. Kasatkin, S. Kühl, M. Hävecker, F. Abild-Pedersen, S. Zander, F. Girgsdies, P. Kurr, B.-L. Kniep, M. Tovar, R. W. Fischer, J. K. Nørskov, and R. Schlögl, Science **336**, 893 (2012).
[4] K. H. Ernst, A. Ludviksson, R. Zhang, J. Yoshihara, and C. T. Campbell, Phys. Rev. B **47**, 13782 (1993).
[5] I. Kasatkin, P. Kurr, B. Kniep, A. Trunschke, and R. Schlögl, Angew. Chem. **119**, 7465 (2007).
[6] O. Dulub, L. A. Boatner, and U. Diebold, Surf. Sci. **504**, 271 (2002).
[7] N.-Y. Topsøe and H. Topsøe, Top. Catal. **8**, 267 (1999).
[8] J. B. Wagner, P. L. Hansen, A. M. Molenbroek, H. Topsøe, B. S. Clausen, and S. Helveg, J. Phys. Chem. B **107**, 7753 (2003).
[9] K. Ozawa, Y. Oba, and K. Edamoto, Surf. Sci. **601**, 3125 (2007).
[10] H. Qiu, F. Gallino, C. Di Valentin, and Y. Wang, Phys. Rev. Lett. **106**, 066401 (2011).
[11] M. Kroll, T. Löber, V. Schott, C. Wöll, and U. Köhler, Phys. Chem. Chem. Phys. **14**, 1654 (2012).
[12] M. Kroll and U. Köhler, Surf. Sci. **601**, 2182 (2007).
[13] P. L. Hansen, J. B. Wagner, S. Helveg, J. R. Rostrup-Nielsen, B. S. Clausen, and H. Topsøe, Science **295**, 2053 (2002).
[14] J. Kiss, J. Frenzel, N. N. Nair, B. Meyer, and D. Marx, J. Chem. Phys. **134**, 064710 (2011).
[15] B. Meyer and D. Marx, J. Phys.: Condens. Matter **15**, L89 (2003).
[16] J. Kossmann, G. Roßmüller, and C. Hättig, J. Chem. Phys. **136**, 034706 (2012).
[17] X. Duan, O. Warschkow, A. Soon, B. Delley, and C. Stampfl, Phys. Rev. B **81**, 075430 (2010).
[18] A. Soon, M. Todorova, B. Delley, and C. Stampfl, Surf. Sci. **601**, 5809 (2007).

[19] A. Soon, M. Todorova, B. Delley, and C. Stampfl, Phys. Rev. B **73**, 165424 (2006).
[20] B. Meyer and D. Marx, Phys. Rev. B **67**, 035403 (2003).
[21] R. Kováčik, B. Meyer, and D. Marx, Angew. Chem., Int. Ed. **46**, 4894 (2007).
[22] M. Valtiner, M. Todorova, G. Grundmeier, and J. Neugebauer, Phys. Rev. Lett. **103**, 065502 (2009).
[23] O. Warschkow, K. Chuasiripattana, M. L. Lyle, B. Delley, and C. Stampfl, Phys. Rev. B **84**, 125311 (2011).
[24] B. Meyer and D. Marx, Phys. Rev. B **69**, 235420 (2004).
[25] J. Tersoff, Phys. Rev. Lett. **56**, 632 (1986).
[26] S. M. Foiles, M. I. Baskes, and M. S. Daw, Phys. Rev. B **33**, 7983 (1986).
[27] M. S. Daw, S. M. Foiles, and M. I. Baskes, Mater. Sci. Rep. **9**, 251 (1993).
[28] T. Hammerschmidt, R. Drautz, and D. G. Pettifor, Int. J. Mater. Res. **100**, 1479 (2009).
[29] D. E. Makarov and H. Metiu, J. Chem. Phys. **108**, 590 (1998).
[30] X. Huang, B. J. Braams, and J. M. Bowman, J. Chem. Phys. **122**, 044308 (2005).
[31] J. Ischtwan and M. A. Collins, J. Chem. Phys. **100**, 8080 (1994).
[32] G. G. Maisuradze, D. L. Thompson, A. F. Wagner, and M. Minkoff, J. Chem. Phys. **119**, 10002 (2003).
[33] A. P. Bartók, M. C. Payne, R. Kondor, and G. Csányi, Phys. Rev. Lett. **104**, 136403 (2010).
[34] M. J. L. Mills and P. L. A. Popelier, Theor. Chem. Acc. **131**, 1137 (2012).
[35] C. M. Handley and P. L. A. Popelier, J. Phys. Chem. A **114**, 3371 (2010).
[36] J. Behler, Phys. Chem. Chem. Phys. **13**, 17930 (2011).
[37] W. McCulloch and W. Pitts, Bull. Math. Biophys. **5**, 115 (1943).
[38] C. M. Bishop, Neural Networks for Pattern Recognition (Oxford University Press, Oxford, 1995).
[39] J. Zupan and J. Gasteiger, Neural Networks in Chemistry and Drug Design: An Introduction (Wiley-VCH, Weinheim, 1999).
[40] G. Cybenko, Math. Contr. Sign. Syst. **2**, 303 (1989).
[41] K. Hornik, M. Stinchcombe, and H. White, Neural Networks **2**, 359 (1989).
[42] D. F. R. Brown, M. N. Gibbs, and D. C. Clary, J. Chem. Phys. **105**, 7597 (1996).
[43] F. V. Prudente, P. H. Acioli, and J. J. S. Neto, J. Chem. Phys. **109**, 8801 (1998).
[44] H. Gassner, M. Probst, A. Lauenstein, and K. Hermansson, J. Phys. Chem. A **102**, 4596 (1998).
[45] L. M. Raff, M. Malshe, M. Hagan, D. I. Doughan, M. G. Rockley, and R. Komanduri, J. Chem. Phys. **122**, 084104 (2005).
[46] M. G. Darley, C. M. Handley, and P. L. A. Popelier, J. Chem. Theor. Comput. **4**, 1435 (2008).
[47] S. Manzhos and T. Carrington, Jr., J. Chem. Phys. **125**, 194105 (2006).
[48] H. T. T. Nguyen and H. M. Le, J. Phys. Chem. A **116**, 4629 (2012).
[49] T. B. Blank, S. D. Brown, A. W. Calhoun, and D. J. Doren, J. Chem. Phys. **103**, 4129 (1995).
[50] S. Lorenz, A. Groß, and M. Scheffler, Chem. Phys. Lett. **395**, 210 (2004).
[51] J. Behler, B. Delley, S. Lorenz, K. Reuter, and M. Scheffler, Phys. Rev. Lett. **94**, 36104 (2005).
[52] J. Ludwig and D. G. Vlachos, J. Chem. Phys. **127**, 154716 (2007).
[53] J. Behler, S. Lorenz, and K. Reuter, J. Chem. Phys. **127**, 014705 (2007).
[54] C. Carbogno, J. Behler, A. Groß, and K. Reuter, Phys. Rev. Lett. **101**, 096104 (2008).
[55] S. Hobday, R. Smith, and J. Belbruno, Model. Simul. Mater. Sci. Eng. **7**, 397 (1999).
[56] S. Hobday, R. Smith, and J. BelBruno, Nucl. Instrum. Methods Phys. Res., B **153**, 247 (1999).
[57] A. Bholoa, S. D. Kenny, and R. Smith, Nucl. Instrum. Methods Phys. Res., B **255**, 1 (2007).
[58] E. Sanville, A. Bholoa, R. Smith, and S. D. Kenny, J. Phys.: Condens. Matter **20**, 285219 (2008).
[59] J. Behler and M. Parrinello, Phys. Rev. Lett. **98**, 146401 (2007).
[60] J. Behler, J. Chem. Phys. **134**, 074106 (2011).
[61] J. Behler, R. Martoňák, D. Donadio, and M. Parrinello, Phys. Rev. Lett. **100**, 185501 (2008).
[62] J. Behler, R. Martoňák, D. Donadio, and M. Parrinello, Phys. Status Solidi B **245**, 2618 (2008).
[63] H. Eshet, R. Z. Khaliullin, T. D. Kühne, J. Behler, and M. Parrinello, Phys. Rev. B **81**, 184107 (2010).
[64] H. Eshet, R. Z. Khaliullin, T. D. Kühne, J. Behler, and M. Parrinello, Phys. Rev. Lett. **108**, 115701 (2012).
[65] R. Z. Khaliullin, H. Eshet, T. D. Kühne, J. Behler, and M. Parrinello, Phys. Rev. B **81**, 100103 (2010).
[66] R. Z. Khaliullin, H. Eshet, T. D. Kühne, J. Behler, and M. Parrinello, Nature Mater. **10**, 693 (2011).
[67] N. Artrith and J. Behler, Phys. Rev. B **85**, 045439 (2012).
[68] K. V. Jovan Jose, N. Artrith, and J. Behler, J. Chem. Phys. **136**, 194111 (2012).
[69] G. C. Sosso, G. Miceli, S. Caravati, J. Behler, and M. Bernasconi, Phys. Rev. B **85**, 174103 (2012).
[70] G. C. Sosso, D. Donadio, S. Caravati, J. Behler, and M. Bernasconi, Phys. Rev. B **86**, 104301 (2012).
[71] G. C. Sosso, J. Behler, and M. Bernasconi, Phys. Status Solidi B **249**, 1880 (2012).
[72] S. Houlding, S. Y. Liem, and P. L. A. Popelier, Int. J. Quantum Chem. **107**, 2817 (2007).
[73] N. Artrith, T. Morawietz, and J. Behler, Phys. Rev. B **83**, 153101 (2011).
[74] T. Morawietz, V. Sharma, and J. Behler, J. Chem. Phys. **136**, 064103 (2012).
[75] V. Blum, R. Gehrke, F. Hanke, P. Havu, V. Havu, X. Ren, K. Reuter, and M. Scheffler, Comput. Phys. Commun. **180**, 2175 (2009).
[76] J. P. Perdew, K. Burke, and M. Ernzerhof, Phys. Rev. Lett. **77**, 3865 (1996).
[77] RuNNer – A Neural Network Code for High-Dimensional Potential Energy Surfaces, Jörg Behler, Lehrstuhl für Theoretische Chemie, Ruhr-Universität Bochum, Germany, 2012.
[78] T. B. Blank and S. D. Brown, J. Chemometr. **8**, 391 (1994).
[79] Electronic supplementary material can be found at www.pss-b.com.
[80] G. Wulff, Z. Kristallogr. Mineral. **34**, 449 (1901).
[81] C. Herring, Phys. Rev. **82**, 87 (1951).
[82] TINKER, Version 5.1, Software Tools for Molecular Design, J.W. Ponder, Biochemistry and Molecular Physics, Washington University, St. Louis, USA, 2011.